

Original Article

Parametric Study of Lateral Earth Pressure on Rigid Retaining Walls Using ABAQUS

Taku Muni¹, Dipika Devi², Sukumar Baishya³

¹Department of Civil Engineering Himalayan University, Jollang, Arunachal Pradesh, India.

^{2,3}Department of Civil Engineering NERIST, Nirjuli, Arunachal Pradesh, India.

²Corresponding Author : dd@nerist.ac.in

Received: 04 December 2024

Revised: 03 January 2025

Accepted: 05 February 2025

Published: 27 February 2025

Abstract - A comprehensive parametric investigation is carried out to explore the effect of the Associative Flow Rule (AFR) and Non-Associative Flow Rule (NAFR) on the behaviour of a rigid retaining wall, particularly concerning the lateral earth pressure exerted on the wall. This analysis is conducted utilizing Finite Element Analysis (FEA) software ABAQUS, which provides a robust platform for studying the interactions and responses within the soil-wall system. The active and passive lateral earth pressure distributions on the wall are obtained for different angles of internal friction (ϕ) with varying dilation angles (ψ). From the analysis, it is found that there is an increasing trend of stability in the results of the distribution of active earth pressure (P_a) with the increase in the value of dilation angle in soil for the same value of ϕ . The passive earth pressure (P_p) distribution results show that the difference in the behaviour of earth pressure due to Associative Flow Rule (AFR) and Non-Associative Flow Rule (NAFR) can be observed only in the lower part of the wall height, while Associative Flow Rule (AFR) in soil with higher value of ϕ may give overestimated passive earth pressure. The earth pressure distribution for the Non-Associative Flow Rule (NAFR) with $\psi=0$ shows more fluctuation and unstable results, whereas $\psi=0.5\phi$ shows more uniform and stable pressure distributions for both passive and active cases. Thus, the study reveals that the dilation angle significantly impacts the behaviour of rigid retaining walls. Hence, a Non-Associative Flow Rule (NAFR) with an appropriate value of dilation angle should be considered in their analysis and design.

Keywords - Earth pressure, Dilation angle, Flow rule, Abaqus, Retaining wall.

1. Introduction

Retaining walls and the associated earth pressure challenges have been integral to civil engineering since its inception. Earth pressure theories given by Coulomb, Rankine and Terzaghi are the earliest analytical studies available with the most basic concept yet conventional in nature [1]. Many researchers have proposed different methods for estimating P_a behind a retaining wall using different analysis methods, but less attention is given to estimating P_p [2]. It has also been known through literature study that conventional methods of analyses, which are still in use, are based on various assumptions. Conventional methods for analyzing earth pressure typically assume an associative plastic flow condition, where the dilation angle (ψ) equals the internal friction angle (ϕ) of the soil. However, it is well-established that plastic flow in soil is inherently non-associative [3-5]. The dilation angle is one of the important soil parameters that control volume change during plastic strain development. It significantly influences various soil structure interaction problems [6, 7]. Researchers like [8-10] incorporated AFR and NAFR in bearing capacity problems using various methods and revealed their significant role in bearing capacity and the

related parameters. Bolton [11] studied the strength and dilatancy of sand and found the dependency of the shearing of dense soil on the rate of dilatancy. He also defined a dilatancy index in terms of relative density and effective stress [12]. Conducted a numerical study to examine the effects of AFR and NAFR on smooth gravity retaining walls. Based on the velocity diagram and earth pressure coefficient value, they concluded that AFR overestimates the magnitude of P_p [13]. conducted a numerical analysis of rigid retaining walls using the FLAC code. From the results of horizontal displacement, it was concluded that NAFR underestimated the passive earth Pressure Coefficient (K_a) and overestimated the active earth Pressure Coefficient (K_p). It was also found that this influence was considerably high for the higher value of ϕ whereas it was not significant for the lower value of ϕ [14]. Carried out numerical simulation of mobilization of P_a behind a retaining wall assuming NAFR, $\psi=0$ and found that soil arching significantly influences the distribution of P_a . Many researchers in the past reported ABAQUS software to be useful for the numerical simulation of earth retaining structures and reported the results obtained to be reliable [15-18]. From the literature review, it is found that many



researchers have carried out studies on dilation angle and its effect on foundation. However, there are limited published research papers addressing earth pressure-related problems. Furthermore, there is no clear comprehension of the relationship between ϕ and ψ that demonstrates its practical application in both associative and non-associative flow rules for predicting reasonable earth pressure behavior in retaining structures. In this paper, an attempt has been made to address this gap by investigating the effects of AFR and NAFR on earth pressure distribution along a gravity retaining wall, employing the Mohr-Coulomb (M-C) plasticity model. In the M-C failure criterion, accurately defining yielding requires determining the effective values of ϕ and cohesion (c), which define the yield surface.

Furthermore, the effective value of ψ must also be evaluated, as it characterizes the potential surface and indicates whether the plastic flow rule is associative ($\psi=\phi$) or non-associative ($\psi\neq\phi$) [4]. The study aims to provide insights into comparing earth pressure distribution for various values of ϕ to understand the prevailing behaviour of earth pressure distribution under the influence of different dilation angles. The practical implication from the present study is that findings will help in understanding the true nature of the behavior of earth pressure distribution for the gravity wall in contrast to the conventional earth pressure distribution and aid in selecting the value of dilation angle, which has a more practical approach.

2. Numerical Modelling

This study performs a two-dimensional plane strain analysis of a gravity retaining wall to examine the impact of associative and non-associative flow rules with increasing values of ϕ on the distribution of P_a and P_p behind the wall. The analysis considers a gravity wall with a height of 3 meters, subjected to a surcharge load of 7 kPa applied to the backfill soil. Figure 1 shows the simplified soil-wall model generated from the assembly module of ABAQUS/CAE. For boundary conditions, the right-hand side of the soil model is prevented from horizontal movement, while vertical movement is allowed. The bottom of the soil model is fixed and prevented from movement from all directions. To handle the stress concentration in the vicinity of the wall, a finer mesh size of 0.3m is used in and around the retaining wall, and a coarse mesh of size 2m is used away from the wall.

Four node linear plane strain quadrilateral element with reduced integration (CPE4R) is used to model both soil and wall. The data for the soil-wall model are adopted from the example problem of [19], which are shown in Table 1. Here, γ (kg/m³) represents the unit weight, E (MPa) represents Young's modulus, and ν represents the poisson's ratio. The concrete gravity wall's behavior is modeled as elastic using an isotropic elastic model, while the soil is represented by the Mohr-Coulomb (M-C) model. In the present study, three basic steps are followed. The first step defines the soil structure

interaction properties, loading conditions, and boundary conditions. In the second step, a gravitational load is applied. The third step is the general static step, where the rate-dependent plasticity and hysteretic behaviour for hyperelastic materials are contemplated. As a part of the analysis, gravity load is initially applied, and the wall is prevented from moving in the lateral direction to simulate the at-rest state. The wall is then moved apart from the retained soil to simulate an active state. Similarly, passive analysis is carried out by allowing the wall to move towards the backfill soil. The results for all these wall conditions are obtained from FEA analysis using ABAQUS/CAE and compared for different values of ϕ and ψ . The evaluation of the rigid retaining wall is conducted by measuring the lateral earth pressure distribution and the plastic strain distribution behind the wall for both active and passive conditions. Three different types of cohesionless backfilled soil are considered with $\phi=34^\circ, 37^\circ, \text{ and } 40^\circ$, respectively. The selected range of ϕ and ψ values in this study was determined based on typical values representing the behavior of dense sand. The earth pressure distribution and plastic strain distribution on the wall are analysed with each backfill soil by considering AFR and NAFR.

Table 1. Properties of soil and concrete (Helwany 2007)

Properties	Soil (Mohr-Coulomb Plasticity)			Retaining wall (Concrete)
γ (kg/m ³)	1700			2300
E (MPa)	182			21300
ν	0.3			0.2
c' (kPa)	0.3			-
ϕ' (deg)	34	37	40	-

Table 2. Cap model parameters adopted (Helwany 2007)

Υ (kg/m ³)	1923
Initial Void Ratio e_0	1.5
Elasticity E(MPa)	182
ν	0.3
Material Cohesion d (Kpa)	10^{-4}
β (deg)	44.56
R	0.2
Initial Yield	0.0
α	0.1
κ	1

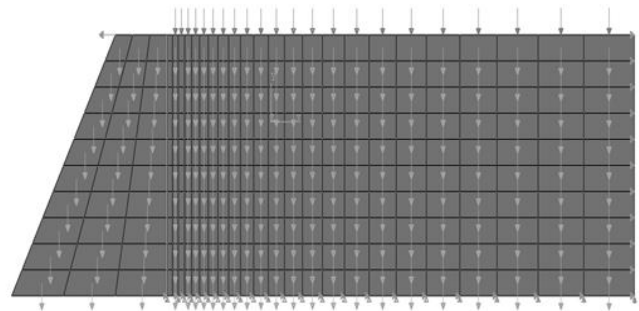


Fig. 1 The soil-wall model

3. Validation and Limitations

To validate the soil-wall model used in the study, two different analyses are carried out using two soil constitutive models, namely, the M-C model and Cap plasticity. The soil parameter values needed for these two models are provided in Table 1 and Table 2, respectively. The earth pressure derived from both the soil constitutive models are compared, and it is found that results from both models give close earth pressure distribution. Figure 2. It shows the relative analysis of earth pressure distribution for two soil models, i.e., the Mohr Coulomb model and Cap Plasticity model, for Figure 2(a) at rest, Figure 2(b) active, and Figure 2(c) passive conditions, respectively. The present study is limited to analysis using only one soil constitutive model, i.e., the M-C model. For the future scope of work, the present numerical study can be further analyzed to develop an empirical relationship between numerical results and theoretical results. This will be a major aid to engineering design for retaining walls and thus enhance its applicability in smart city development.

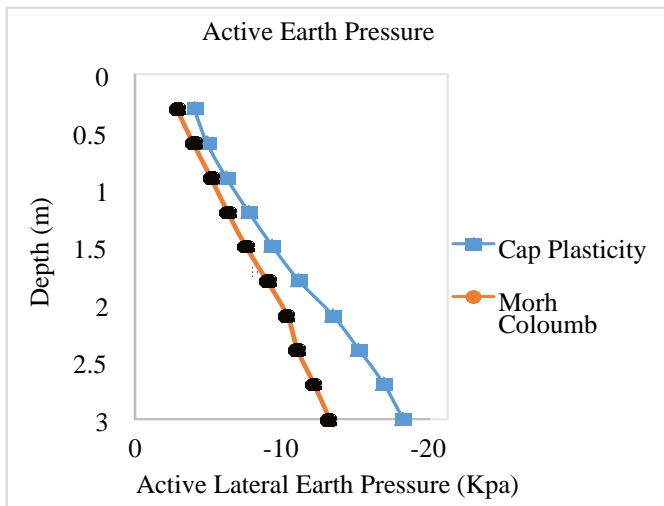


Fig. 2(a) Comparison of at-rest earth pressure distribution

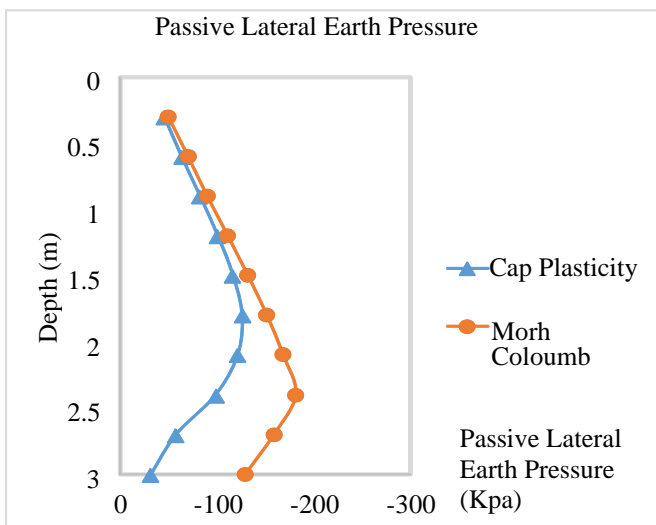


Fig. 2(b) Comparison of P_p distribution

4. Results and Discussion

The results for the present two-dimensional plane strain analysis on the gravity retaining wall are presented for earth pressure distribution and plastic strain distribution throughout the entire depth of the wall section.

Figure 3(a) presents the active earth pressure distribution diagrams for three different cohesionless backfill soils with $\phi = 34^\circ, 37^\circ,$ and 40° respectively, for analysis done with NAFR considering dilation angle $\psi = 0$.

It can be observed from Figure 3(a) that active earth pressure distribution for this analysis shows more fluctuation and unstable patterns of behaviour along the wall depth. It can also be noted that P_a at the wall's lower section decreases nonlinearly as the value of ϕ increases from 34° to 40° .

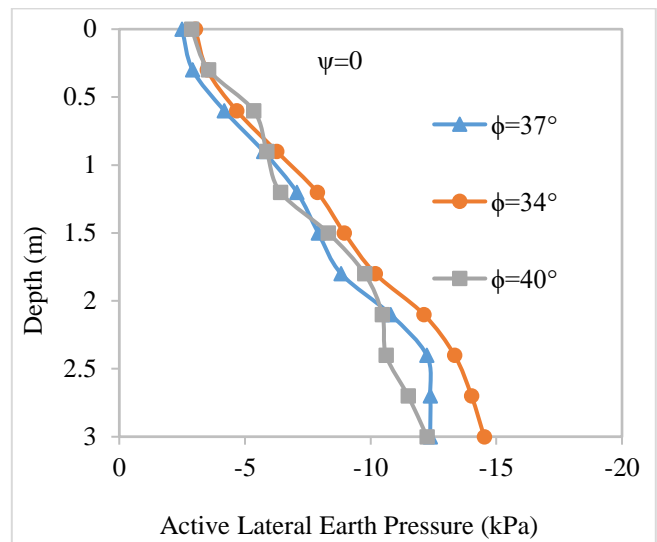


Fig. 3(a) Comparison of the distribution of P_a for three different soils with $\psi = 0$

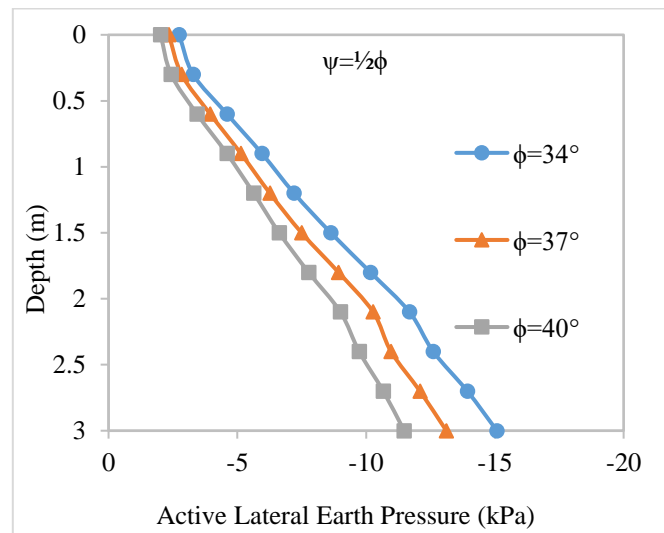


Fig. 3(b) Comparison of the distribution of P_a for three different soils with $\psi = \phi/2$

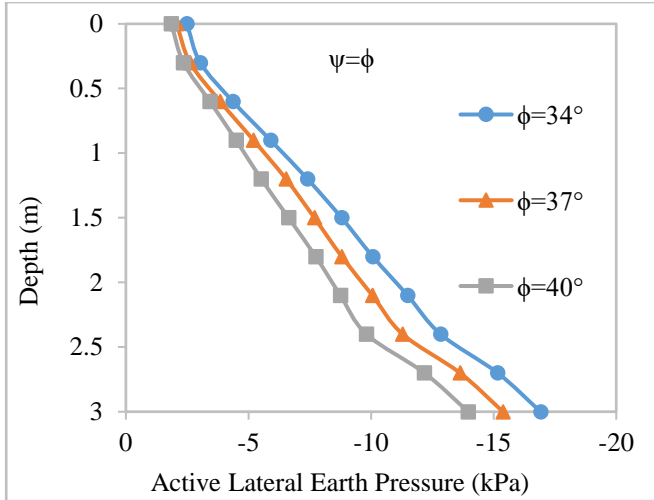


Fig. 3(c) Comparison of the distribution of P_a for three different soils with $\psi = \phi$

Figure 3(b) represents the active pressure distribution diagrams of three types of cohesionless backfill soils ($\phi = 34^\circ$, 37° , and 40°) for analysis done with NAFR considering dilation angle $\psi = \frac{1}{2}\phi$. The results of the analysis with the same soils with AFR ($\psi = \phi$) are shown in Figure 3(c). The distributions of P_a with these two dilation angles are more uniform and stable. It can also be observed that in contrast to the results with $\psi = 0$, the value of P_a at the wall base decreases linearly with the increased value of the ϕ of the backfill soil for both the cases with $\psi = \frac{1}{2}\phi$ and $\psi = \phi$. Similar behaviour for load-displacement curves with AFR and NAFR was reported by (Benmeddour et al. 2012). The analysis results for the distribution of P_a with increasing values of ψ are also compared in Figure 4(a) for backfill soil with $\phi = 34^\circ$. Similarly, Figures 4(b) and 4(c) represent the distribution of the P_a results with increasing values of ψ for backfill soils with $\phi = 37^\circ$ and 40° respectively.

Another observation that can be made from these results of active pressure distribution illustrated in Figures 4(a), 4(b) and 4(c) is that as the dilation angle ψ increases, the fluctuation of the active pressure distribution curves decreases. This means there is an increasing order of stability in the results of active pressure distribution with an increasing value of dilation angle ψ in soil for the same value of ϕ .

The results also indicate that fluctuations in the active pressure distribution with depth are observed in analyses using an NAFR when $\psi = 0$. Soils with a higher value of ϕ prominently exhibit greater fluctuations in earth pressure distribution. Figures 5(a), 5(b) and 5(c) represent the plastic strain distribution behind the rigid retaining wall for three different dilation angles during the active state for analysis done with backfill soil having $\phi = 34^\circ$. These figures clearly indicate the development of wedge-shaped failure zones with linear failure surfaces crossing the heel of the wall in each case of the analysis.

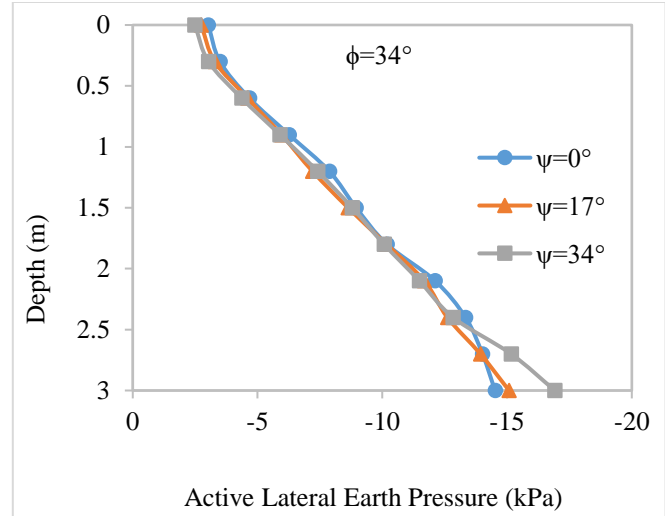


Fig. 4(a) Comparative study of P_a distribution for $\phi = 34^\circ$ and three values of ψ

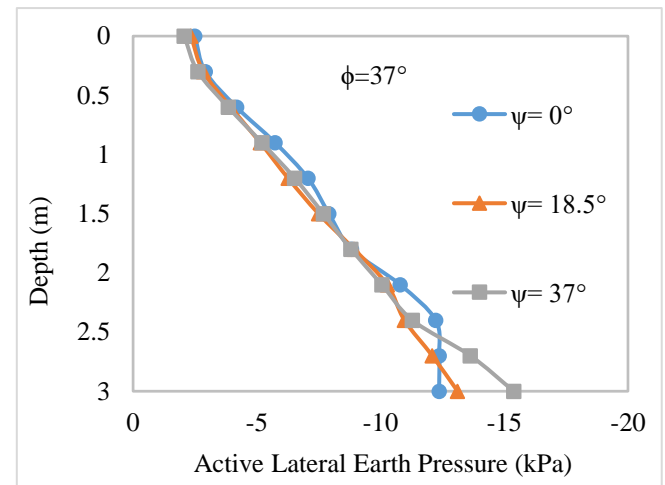


Fig. 4(b) Comparative study of P_a distribution for $\phi = 37^\circ$ and three values of ψ

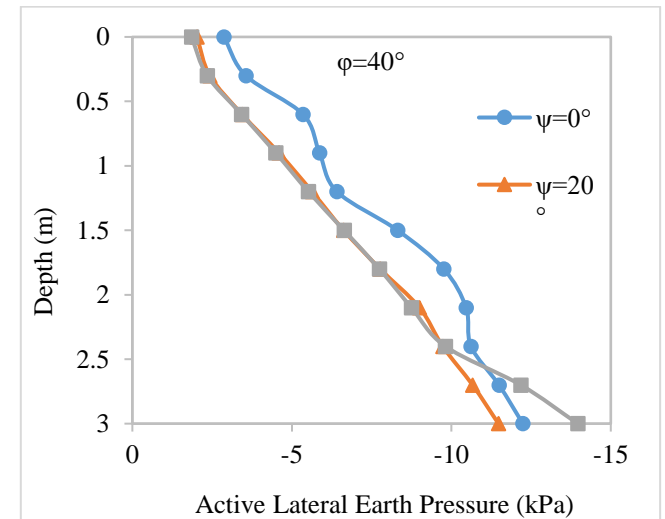


Fig. 4(c) Comparative study of P_a distribution for $\phi = 40^\circ$ and three values of ψ

A visual comparison of these figures (Figures 5(a), 5(b) and 5(c)) also reveals that the failure zone becomes more prominent and smaller in size for AFR ($\phi = \psi$). It is also observed that the magnitude of plastic strains at the top of the wall increases with rising dilation angle. Similar patterns were observed from the retaining wall analysis with the other two categories of backfill soil, for which figures are not included for the brevity of the paper's presentation.

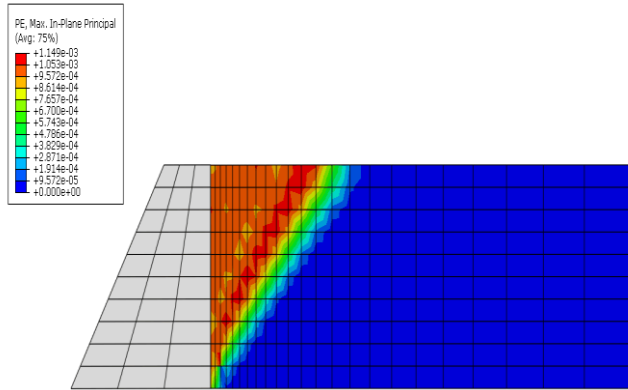


Fig. 5(a) Plastic strains distribution behind the wall in active state for $\phi = 34^\circ$ and $\psi = 0$

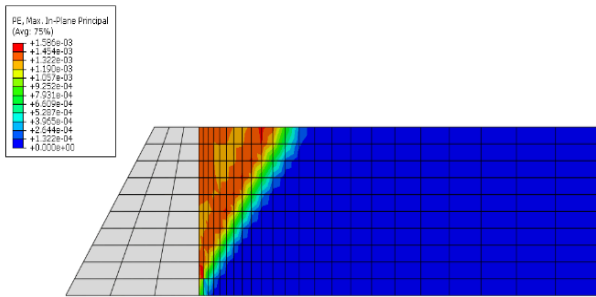


Fig. 5(b) Plastic strains distribution behind the wall in active state for $\phi = 34^\circ$ and $\psi = \frac{1}{2}\phi$

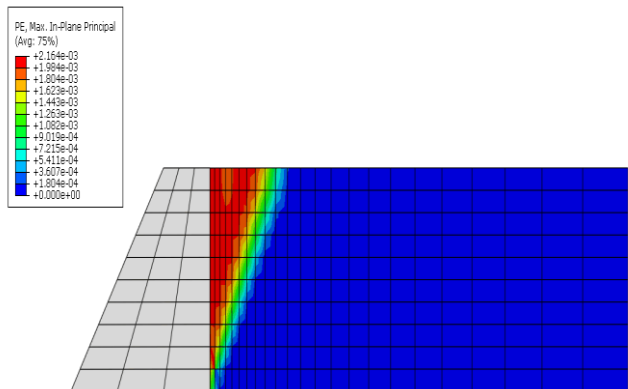


Fig. 5(c) Plastic strains distribution behind the wall in active state for $\phi = 34^\circ$ and $\psi = \phi$

Figure 6(a) presents the distribution of the Pp for three different backfill soils with $\phi = 34^\circ, 37^\circ$, and 40° respectively for analysis done with NAFR considering $\psi=0$.

A similar pattern of results is obtained with $\psi = \frac{1}{2}\phi$ and $\phi = \phi$ for all three types of backfill soil, which are presented in Figures 6(b) and 6(c). From the results of the pressure distributions for the passive case shown in Figures 6(a), 6(b), and 6(c), it is noted that the pressure distribution is significantly more consistent compared to that of the active case. It also can be commented that the stability of the earth pressure distribution is more prominent in the analysis with the associated flow rule, $\psi = \phi$. Small fluctuation can be observed in the results of the NAFR, especially at the base of the wall.

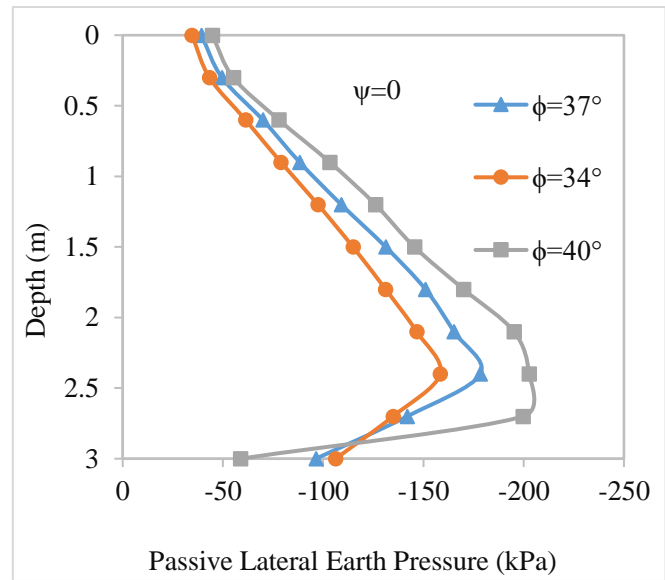


Fig. 6(a) Comparative study of Pp distribution for three types of soils with $\psi=0$

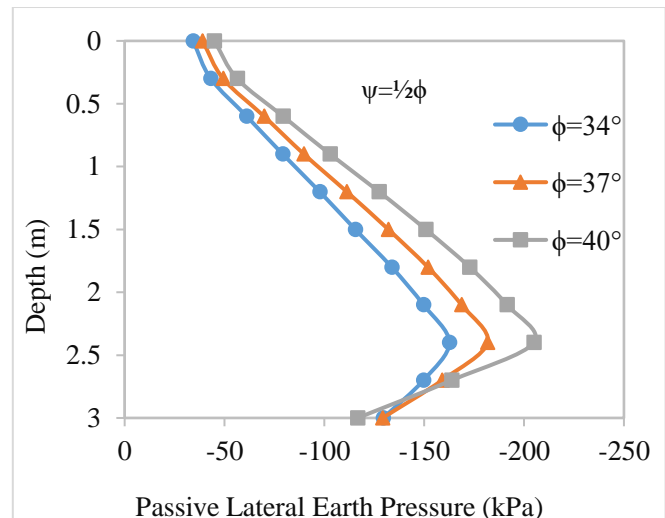


Fig. 6(b) Comparative study of Pp distribution for three types of soils with $\psi = \phi/2$

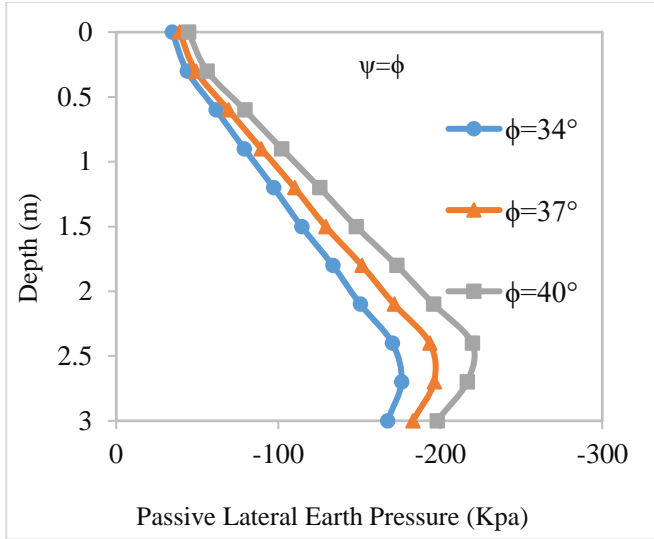


Fig. 6(c) Comparative study of P_p distribution for three types of soils with $\psi = \phi$

The results of the distribution of P_p on the back of the wall are also compared concerning the variation of the values of ψ . Figures 7(a), 7(b) and 7(c) present these results for the analysis done with three different backfill soils. From the results, it is quite clear that the distributions of P_p for different values of ψ with AFR or NAFR behave similarly up to about two-thirds of wall height before reaching the ultimate values of P_p . Only after reaching the ultimate value of P_p the noticeable difference in behaviour due to different dilation angles can be observed. Another observation made in Figures 7(a), 7(b) and 7(c) is that the ultimate value of P_p seems to increase as the value of ψ is increased, and this phenomenon is seen for all the values of ϕ . The percentage of increment of ultimate earth pressure is higher for soil with a higher value of ϕ . So, it can be commented that AFR, especially in soil with a higher value of ϕ , may give an overestimated value of P_p .

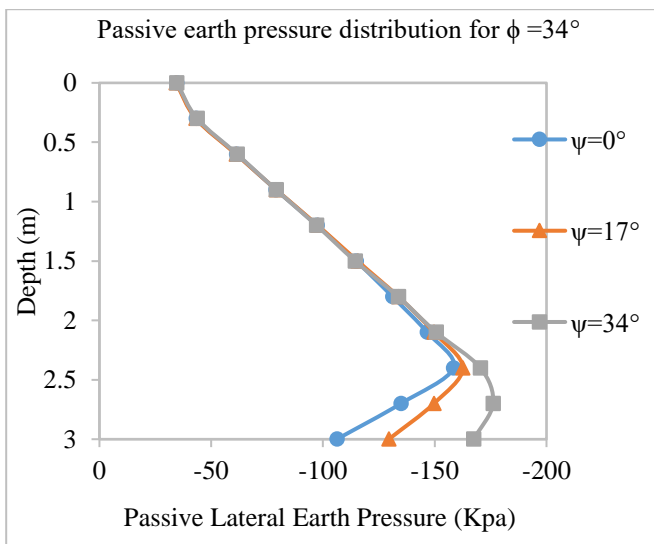


Fig. 7(a) Comparison of the distribution of P_p for soil with $\phi = 34^\circ$ and three values of ψ

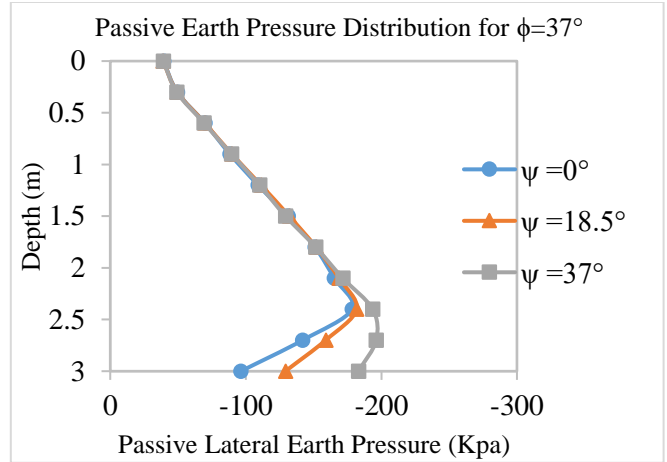


Fig. 7(b) Comparison of the distribution of P_p for soil with $\phi = 37^\circ$ and three values of ψ

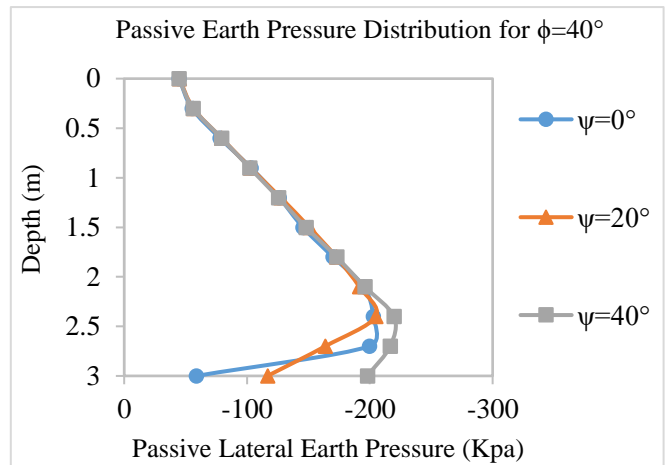


Fig. 7(c) Comparison of the distribution of P_p for soil with $\phi = 40^\circ$ and three values of ψ

Figures 8(a), 8(b) and 8(c) represent the plastic strain distribution behind the retaining wall during the passive state for three different dilation angles for soil with $\phi = 34^\circ$. In all three scenarios, the failure surface extends through the heel of the wall. In this case, unlike the active state, the failure zone becomes more prominent and smaller in size for NAFR with $\psi = 0$. Similar patterns were observed for the other two soil types.

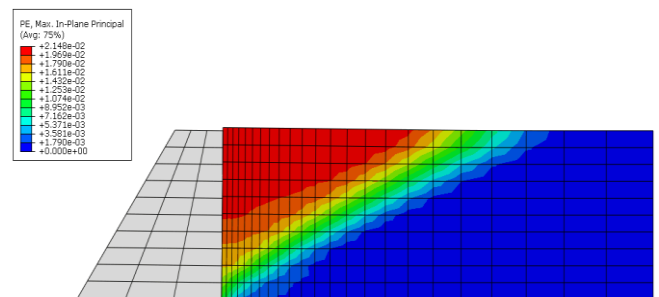


Fig. 8(a) Plastic strains distribution behind the wall in a passive state for $\phi = 34^\circ$ and $\psi = 0$

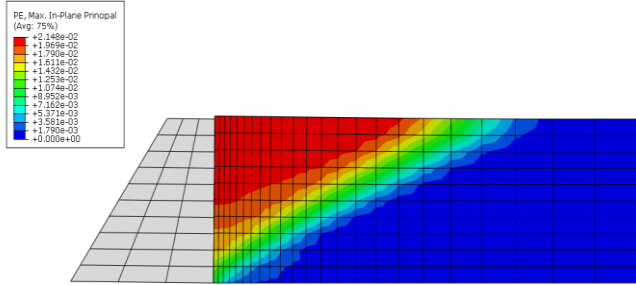


Fig. 8(b) Plastic strains distribution behind the wall in a passive state for $\phi = 34^\circ$ and $\psi = \phi/2$

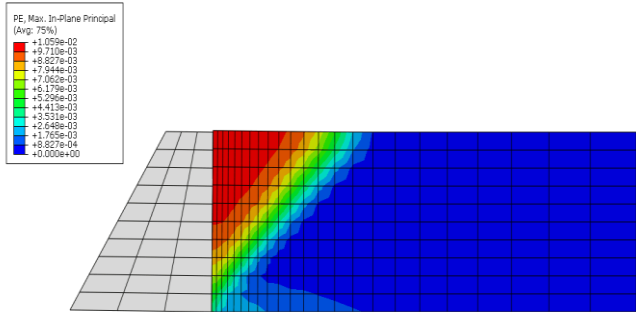


Fig. 8(c) Plastic strains distribution behind the wall in a passive state for $\phi = 34^\circ$ and $\psi = \phi$

5. Conclusion

The present numerical analysis was conducted to examine the behavior of a gravity retaining wall subjected to varying ϕ values, considering both AFR and NAFR. The following general observations are made based on the analysis:

5.1. Active Earth Pressure (P_a) Distribution

The results indicate that the NAFR with a dilation angle of $\psi = 0$ exhibits greater fluctuations and less stable earth pressure distribution. In contrast, the NAFR with $\psi = \frac{1}{2}\phi$ and

the AFR with $\psi = \phi$ yield more uniform and stable distributions. As the dilation angle ψ increases, the stability of the earth pressure distribution curves improves. This suggests that, for the same internal friction angle (ϕ), higher dilation angles result in more stable P_a outcomes.

5.2. Passive Earth Pressure (P_p) Distribution

The P_p distribution shows similar behaviour across different dilation angles, whether associative or non-associative, up to approximately two-thirds of the wall height before reaching the ultimate earth pressure. Variations in P_p due to dilation angle become noticeable only after the ultimate pressure is reached.

The ultimate P_p increases with higher dilation angles, with the increase being more pronounced in soils with higher internal friction angles. Consequently, the AFR may overestimate P_p , particularly in soils with higher ϕ values.

5.3. Optimal Dilation Angle

The parametric study, conducted for three different dilation angles, indicates that a dilation angle equal to half the internal friction angle ($\psi = \frac{1}{2}\phi$) provides the most reasonable earth pressure results.

Acknowledgements

The authors would like to acknowledge and sincerely thank the organizing committee of the International Conference on Computer-Aided Modeling for the Sustainable Development of Smart Cities (CAMSSC), sponsored by the Anusandhan National Research Foundation (ANRF), held at the Department of Civil Engineering, North Eastern Regional Institute of Science and Technology (NERIST), Nirjuli, Arunachal Pradesh, India, during November 27-30, 2024, for allowing us to present the paper and sponsoring the paper for publication.

References

- [1] Chuanxiang Xiong et al., "Active Earth Pressure of Narrow Cohesionless Backfill on Balance Weight Retaining Walls Rotating about the Bottom," *Structures*, vol. 67, 2024. [CrossRef] [Google Scholar] [Publisher Link]
- [2] Tarek Khelifa, Housseem Eddine Lanabi, and Sadok Benmebarek, "Passive Earth Pressure due to Surcharge Loading under Three Modes of Wall Movement," *International Journal of Geotechnical Engineering*, vol. 18, no. 2, pp. 150-163, 2024. [CrossRef] [Google Scholar] [Publisher Link]
- [3] K. Krabbenhoft, "Static and Seismic Earth Pressure Coefficients for Vertical Walls with Horizontal Backfill," *Soil Dynamics and Earthquake Engineering*, vol. 104, pp. 403-407, 2018. [CrossRef] [Google Scholar] [Publisher Link]
- [4] K. Magdalena, "Influence of the Ratio Between Dilatancy Angle and Internal Friction Angle on Stress Distribution Behind a Gravity Retaining Wall," *Architecture Civil Engineering Environment*, vol. 8, no. 1, pp. 77-82, 2015. [Google Scholar]
- [5] Christoph Schmüdderich, Franz Tschuchnigg, and Helmut F. Schweiger, "Significance of Flow Rule for the Passive Earth Pressure Problem," *Acta Geotechnica*, vol. 17, pp. 81-92, 2022. [CrossRef] [Google Scholar] [Publisher Link]
- [6] Mehdi Veiskarami, Jyant Kumar, and Fatemeh Valikhah, "Effect of the Flow Rule on the Bearing Capacity of Strip Foundations on Sand by the Upper-Bound Limit Analysis and Slip Lines," *International Journal of Geomechanics*, vol. 14, no. 3, 2014. [CrossRef] [Google Scholar] [Publisher Link]
- [7] Yifei Sun, Yufeng Gao, and Yang Shen, "Non-Associative Fractional-Order Bounding-Surface Model for Granular Soils Considering State Dependence," *International Journal of Civil Engineering*, vol. 17, pp. 171-179, 2019. [CrossRef] [Google Scholar] [Publisher Link]

- [8] Ouassim Rahmouni et al., “Numerical Study of the Bearing Capacity of a Strip Footing Near of Geosynthetic-Reinforced Soil Retaining Walls,” *4th International Conference on New Developments in Soil Mechanics and Geotechnical Engineering*, pp. 1-6, 2016. [[Google Scholar](#)]
- [9] Koushik Halder, Debarghya Chakraborty, and Sujit Kumar Dash, “Bearing Capacity of a Strip Footing Situated on Soil Slope Using a Non-Associated Flow Rule in Lower Bound Limit Analysis,” *International Journal of Geotechnical Engineering*, vol. 13, no. 2, pp. 103-111, 2019. [[CrossRef](#)] [[Google Scholar](#)] [[Publisher Link](#)]
- [10] K. Halder, and D. Chakraborty, “Bearing Capacity of a Strip Footing Situated on Reinforced Cohesionless Soil Slope Using Non-Associated Flow Rule,” *Geo-Congress 2019: Geotechnical Materials, Modeling, and Testing*, 2019. [[CrossRef](#)] [[Google Scholar](#)] [[Publisher Link](#)]
- [11] M.D. Bolton, “The Strength and Dilatancy of Sands,” *Geotechnique*, vol. 36, no. 1, pp. 65-78, 1986. [[CrossRef](#)] [[Google Scholar](#)] [[Publisher Link](#)]
- [12] Jim Shiau, and Catherine Smith, “Numerical Analysis of Passive Earth Pressures with Interfaces,” *Proceedings of the III European Conference on Computational Mechanics*, 2006. [[CrossRef](#)] [[Google Scholar](#)] [[Publisher Link](#)]
- [13] D. Benmeddour et al., “Numerical Study of Passive and Active Earth Pressures of Sands,” *Computers and Geotechnics*, vol. 40, pp. 34-44, 2012. [[CrossRef](#)] [[Google Scholar](#)] [[Publisher Link](#)]
- [14] A. Sadrekarimi, and S. Damavandinejad Monfared, “Numerical Investigation of The Mobilization of Active Earth Pressure on Retaining Walls,” *Proceedings of the 18th International Conference on Soil Mechanics and Geotechnical Engineering*, Paris, France, pp. 793-796, 2013. [[Google Scholar](#)] [[Publisher Link](#)]
- [15] Fan Cai, “Finite Element Modeling of Mechanical Behavior of Geogrid Reinforced Soil Retaining Walls,” *Proceedings of the Indian National Science Academy*, pp. 1-14, 2024. [[CrossRef](#)] [[Google Scholar](#)] [[Publisher Link](#)]
- [16] K. Senthil, M.A. Iqbal, and Amit Kumar, “Behavior of Cantilever and Counterfort Retaining Walls Subjected to Lateral Earth Pressure,” *International Journal of Geotechnical Engineering*, vol. 8, no. 2, pp. 167-181, 2014. [[CrossRef](#)] [[Google Scholar](#)] [[Publisher Link](#)]
- [17] Liang Tang et al., “Finite Element Analysis of Lateral Earth Pressure on Sheet Pile Walls,” *Engineering Geology*, vol. 244, pp. 146-158, 2018. [[CrossRef](#)] [[Google Scholar](#)] [[Publisher Link](#)]
- [18] Zheng Hu et al., “Active Earth Pressure Acting on Retaining Wall Considering Anisotropic Seepage Effect,” *Journal of Mountain Science*, vol. 4, pp. 1202-1211, 2017. [[CrossRef](#)] [[Google Scholar](#)] [[Publisher Link](#)]
- [19] Sam Helwany, *Applied Soil Mechanics with ABAQUS Applications*, Wiley, pp. 1-385, 2007. [[Google Scholar](#)] [[Publisher Link](#)]